

UPCommons

Portal del coneixement obert de la UPC

<http://upcommons.upc.edu/e-prints>

This is an Accepted Manuscript of an article published by Taylor & Francis in
International Journal of Remote Sensing on October 4 2020, available online:
<https://doi.org/10.1080/01431161.2020.1798548>.

Laboratory-based spectral data acquisition of roof materials

Perla Zambrano-Prado^{*a, b}, Alejandro Josa^c, Joan Rieradevall^{a, d}, Fernando Pérez^e, Juan Marchan^e, Santiago Gassó^f, Xavier Gabarrell^{a, d}

^aSostenipra Research Group (Sostenipra 2017 SGR 1683), Institut de Ciència I Tecnologia Ambientals (ICTA-UAB), Universitat Autònoma de Barcelona, Barcelona Spain.

^bDepartment of Techniques and Construction, Art, Architecture, and Design University Center, (CUAAD), University of Guadalajara (UdG), Guadalajara, México

^cDepartment of Civil and Environmental Engineering (DECA), Civil Engineering School (Escola de Camins), Universitat Politècnica de Catalunya - BarcelonaTech (UPC), Barcelona, Spain.

^dDepartment of Chemical and Biological Environmental Engineering, Universitat Autònoma de Barcelona (UAB), Barcelona, Spain.

^eÀrea d'Observació de la Terra – PCOT, Institut Cartogràfic i Geològic de Catalunya, (ICGC) Barcelona, Spain.

^fDepartment of Projects and Construction Engineering, Universitat Politècnica de Catalunya BarcelonaTech (UPC), Barcelona, Spain.

ORCiDs

Perla Zambrano 0000-0001-5911-3585

Alejandro Josa 0000-0003-1180-7910

Joan Rieradevall 0000-0003-3360-6829

Santiago Gassó 0000-0003-0481-4522

Xavier Gabarrell 0000-0003-1730-4337

Perla Zambrano-Prado Sostenipra Research Group (Sostenipra 2017 SGR 1683),
Institut de Ciència I Tecnologia Ambientals (ICTA-UAB), Universitat Autònoma de
Barcelona, 08193 Cerdanyola del Vallès, Barcelona, Spain. e-mail:
perla.zambrano@uab.cat

Laboratory-based spectral data acquisition of roof materials

Abstract

Roof characteristics such as material type and their properties information are essential to integrating urban agriculture (UA), rainwater harvesting (RWH), and energy systems on roofs. Roof materials can be identified from their spectral signatures. However, this identification requires a priori knowledge of the materials' spectral characteristics. The main perspective of this work is the future use of spectral data for roof classification. A common practice in mapping materials is the use of spectral libraries. In this regard, this work describes a novel framework for laboratory-based spectral data acquisition. The reflectance data of common, recently introduced (plastics and metals), and representative roof materials from the Mediterranean region were obtained. Data acquisition was conducted in a laboratory under controlled conditions using a high-spatial-resolution (HSR) sensor, which is usually used for airborne surveys. Large variations in the spectral reflectance data were observed due to the composition of the roof material. Flat spectral signatures were found for fibre cement, concrete, gravels and some metals, especially from the near-infrared (NIR) spectral region. Colour and surface finish greatly influence the visible (VIS) spectral range. It was confirmed that the view angle did not modify the spectral shapes. A collection of 39 spectral data of roof materials (ceramics, concrete, fibre cement, metals, plastics, paints, stone, and wood) were compiled into a spectral library that is available online.

1. Introduction

To supply essential needs, such as food, water, and energy, to citizens, cities must depend on their surrounding areas. According to the United Nations, by 2050, 68% of the world's population will live in cities (United Nations 2018). The global demand for food, water, and energy is estimated to increase by over 50% (IRENA 2015). In this context, urban agriculture (UA), rainwater harvesting systems (RWHS), and renewable energy systems are key strategies for producing local resources and supplying these essential needs.

Roofs represent half of the total impervious surface in cities and are generally unused spaces. Rooftops can be used for growing food, collecting rainwater, and generating energy (e.g., solar photovoltaic (PV) or solar thermal panels). Roof characteristics (i.e., the geometry, area, slope, solar radiation and material) are essential data for assessing their suitability for integrating food, water, or energy (FWE) production systems in cities (Villarreal and Dixon 2005; Carter and Keeler 2008; Orsini et al. 2016; Toboso-Chavero et al. 2018).

Roof information has traditionally been conducted through ground-level measurement techniques. However, these techniques are inefficient, time consuming, and impractical for obtaining roof information on large scales. In this sense, new methods are needed to obtain roof information properties, and remote sensing (RS) technology represents an efficient and advantageous tool to obtain information at large scales about impervious surfaces such as roads, sidewalks, and roofs (Samsudin, Shafri, and Hamedianfar 2016).

1.1 Remote sensing and roof data collection

Remote sensing refers to the technology to acquire data in relation to an object without being in physical contact (Arnold and Gibbons 1996). RS technology such as light detection and ranging (LiDAR) and imagery systems have been used for obtaining roof properties to assess the suitability to integrate UA, RWHS, and PV systems in cities.

1.1.1 LiDAR systems

LiDAR systems are active RS that focus on geometry rather than radiometry (Weng 2012). These sensors have been used to create digital elevation models (DEMs) and digital surface models (DSMs) (Wang and Wang 2011). LiDAR technology can provide precise information about elements in an urban area such as buildings and trees (Martín,

Domínguez, and Amador 2015). Compared with other sources of data, such as conventional imagery, LiDAR has many advantages, short processing time and can acquire 3D information over target areas by mostly automated operation (Weng 2012).

LiDAR and UA. Berger (2013) analysed the potential of rooftop agriculture in New York City using LiDAR data. These data allowed the identification of roof characteristics such as surface area and slope to assess the feasibility of integrating rooftop UA systems. Saha and Eckelman (2017) described an automated procedure combining geographic information systems (GIS) and LiDAR data to quantify suitable areas for UA at ground level and on rooftops. A DSM of Boston buildings was created using a remotely sensed LiDAR point cloud dataset. From this DSM, the roof area and slope were obtained to identify potential roof areas for UA. Nadal et al. (2017) used LiDAR data acquired with a Leica ALS50-II airborne sensor. Roof characteristics such as surface, solar radiation, and slope were obtained. These data allowed the identification and assessment of roof potential to integrate UA in industrial buildings in Barcelona.

LiDAR and RWHS. Few works have been performed to identify suitable roofs to integrate RWHS. Grant, McKinney, and Ries (2017) used LiDAR data to identify rooftop surfaces. LiDAR data allowed calculation of the catchment area of the rooftop and the potential for RWHS in Florida (USA). Lupia et al., (2017) analysed the water savings through RWHS from building rooftops to irrigate fruit and vegetable crops in the urban area of Rome, Italy. Data of rooftops areas were obtained from LiDAR data, and then the total roof surface was analysed to quantify rainwater collection. Oyedayo (2018) provided a novel framework for understanding the spatiotemporal pattern of rooftop rainwater harvesting potential in the Taita Hills region (Kenia), providing decision support for RWHS implementation. LiDAR data were used to automatically

generate the footprints of roofs, and roof polygons were generated from the LiDAR data to estimate the rooftop rainwater harvesting potential for domestic water needs in the region. LiDAR data were obtained through two campaigns, the first in 2013 using the Optech ALTM 2100 sensor and the second in 2015 with Leica ALS60.

LiDAR and PV. Several works used GIS and remote sensing LiDAR data to quantify solar PV potential on roofs (Palmer et al. 2018). Margolis et al. (2017) used LiDAR data obtained from the US Department of Homeland Security. The data were processed to determine the shading, tilt, and azimuth of each rooftop at a horizontal resolution of 1 m². A set of criteria was then applied to determine whether roof areas were suitable for PV systems. Nguyen et al. (2012) assessed PV rooftop solar potential in Kingston (Canada) using an Optech Airborne Laser Terrain Mapper 3100 (LiDAR system).

Potential rooftops for PV systems were identified, and a calculation of the total potential area was performed. Brito, Gomes, Santos, and Tenedório (2012) estimated the PV roof potential in Carnaxide (Portugal) using building footprints acquired from LiDAR data, and an ArcGIS extension was used for modelling roof solar radiation. The results showed a potential capacity to cover 48% of the local electricity demand. Kodysh, Omitaomu, Bhaduri, & Neish, (2013) estimated solar potential on rooftops, for 212,000 buildings in Knox County, Tennessee, (USA). The methodology allows the identification of suitable roofs with higher potentials for installing PV systems. The work was performed using LiDAR, building footprint data and GIS. Bayrakci Boz, Calvert, and R. S. Brownson (2015) acquired LiDAR data and building footprints to obtain roof characteristics (slope, azimuth, and shading) to identify rooftops suitable for solar energy systems. The case study was the city of Philadelphia, USA. The results showed that 33.7% of the building footprint areas were suitable for PV systems.

Through the previous review, we can observe that to assess the feasibility of rooftop UA, only a few works have used LiDAR technology, most of which are located in the USA. All studies obtained roof area and slope data from LiDAR to identify minimum surface requirements and the presence of flat roofs to integrate rooftop UA and quantify their potential.

To identify suitable areas for RWHS, few works have used LiDAR data; in these cases, roof areas were used to calculate the total rainwater that can be collected. These works were performed in Europe, the USA and Africa.

In contrast to the previous areas of application (UA and RWHS), the use of LiDAR data has been widely used for PV potential. Geometric data of the roofs, such as area, slope, and azimuth, were used to identify and calculate solar potential. Most of these works have been developed in the USA, but there are also case studies in Canada and Europe.

All these works identified geometric roof characteristics (slope and surface area), shadows and solar access, which are essential roof properties to assess the potential integration of FWE systems. However, LiDAR technology does not have the capability to identify roof materials.

1.1.2 Imagery systems

Imagery systems are passive remote sensors that record the radiation either reflected or emitted by surfaces. Imagery systems operate in a wide spectral range from visible (VIS), near-infrared (NIR), shortwave infrared (SWIR) and thermal-infrared (TIR) (Liu and Mason 2009).

Data acquired from multispectral imagery commonly consist of 3 to 7 bands (e.g., Landsat satellite) of data and have bandwidths ranging from 50 to 120 or more nanometres (nm) (Hermiyanty, Wandira Ayu Bertin 2017). Imaging spectrometers, also

called hyperspectral remote sensors, are a revolutionary development in imagery systems. These systems have approximately 100 to 200 or more spectral bands with relatively narrow bandwidths (5-10 nm) (Shafri et al. 2012; Liu and Mason 2009).

Imaging systems and UA. Nadal et al. (2017) used hyperspectral data acquired from a Thermal Airborne Spectrographic Imager 600 (TASI-600) to identify the following roof materials: metal, gravel, concrete, and fibre cement. The data were used to assess the potential implementation of rooftop greenhouses for growing food in Barcelona, Spain. Other work by Nadal et al. (2019) used orthophotos from a satellite to assess UA potential on residential buildings in Quito (Ecuador). Orthophotos were used to identify roof areas, and these areas were digitalized as polygons to quantify the total roof potential to integrate UA.

Imaging systems and RWHS. Ojwang, Dietrich, Anebagilu, Beyer, and Rottensteiner (2017) used high-spatial-resolution imagery (WorldView-2 satellite) to detect roof areas and materials to integrate RWHS in Mombasa (Kenya). Roof materials, tiles, iron and concrete were detected using supervised image classification, and a total roof area of 3 km² was identified as suitable for RWHS. Radzali et al. (2018) used WorldView-3 satellite imagery to obtain spectral and spatial information of roofs. Three types of roofing material were identified in the study area: concrete, metal, and asbestos; in addition, the condition (new or old) of the roof was identified. This assessment was done by the true colour combination of band 5, band 3, and band 2 of the World-View 3 image. The results allowed the identification and quantification of roofs to integrate RWH in Seri Kembangan, Malaysia.

Imaging systems and PV. Jamal et al. (2014) mapped the potential roof area available in Dhaka (Bangladesh) and evaluated the possible electricity supply from rooftop PV

systems. To perform the estimation, Quickbird satellite imagery and GIS tools were used. The results showed that PV generation potential might meet 15% of local grid electricity demands. Singh and Banerjee (2015) used a combination of land use data and GIS-based satellite image analysis for the estimation of rooftop PV potential in Mumbai (India). The results showed that rooftop PV potential might provide from 12.8 to 20% of the average daily energy demand. Khan and Arsalan (2016) used GIS and satellite imagery acquired from Google Earth™ to identify the available rooftop area for PV potential. The case study was performed in Karachi (Pakistan). Solar power potential and annual energy outputs for different scenarios of PV technologies were computed. The results demonstrated that monocrystalline and amorphous Si-based rooftop PV systems could provide 122.4% and 65.2% of the peak power demand, respectively.

As we can observe, imagery systems have rarely been used to identify roof properties for UA implementation purposes. However, through these systems, it is possible to obtain roof material information for integrating UA rooftops.

Few works have used imagery systems to obtain information on roofing materials and roofing conditions to assess the potential of RWHS. However, most of the studies used imagery systems to identify roof areas without considering roof materials.

There have been many studies conducted by different researchers around the globe that demonstrated the use of GIS tools and RS data (multi- or hyperspectral) for the identification and estimation of rooftop PV (Khan and Arsalan 2016). However, there is no research about the identification of roof materials with the purpose of assessing the feasibility of PV systems.

In conclusion, hyperspectral data obtained by imaging spectrometers provide the potential to derive detailed information on the properties of different surface materials (Arnold and Gibbons 1996), in contrast to LiDAR systems that provide information

about the height and geometric properties of roofs, while high-resolution images can provide information about spectral signatures.

Most of the works developed to identify roof characteristics to integrate FWE systems centre their interest on the slope, surface area, shadows and solar access. Therefore, there is a gap in the identification of roof materials to assess the potential integration of FWE systems. Roof materials are essential data to integrate into these systems: if a roof does not have the necessary load-bearing capacity to support the weight of an FWE system, it will not be possible to install a system on it. In this sense, spectral characteristics are useful for mapping materials, and from this knowledge, an indicator of the construction systems in a given area can be obtained, and the load capacity of roofs can be estimated. Furthermore, the quality and quantity of rainwater harvested from roofs are significantly affected by roofing materials (Farreny et al. 2011; Sanyé-Mengual et al. 2015; Nadal et al. 2017).

1.1.2 Spectral libraries of impervious materials

Roof materials can be classified from their spectral signatures (Jilge et al. 2017); however, the large number of different materials and their spectral variations are a challenge for roof classification. In this sense, a priori knowledge of the spectral characteristics of the materials is required (Ben-Dor, Levin, and Saaroni 2001; Heiden et al. 2001; Kotthaus et al. 2014).

A common practice in mapping materials is to use spectral libraries (Nidamanuri and Ramiya 2014) that provide information about the spectral characteristics of materials. Spectral data can be acquired at three scales: in the laboratory, in the field, or from remote sensing platforms (Stevens et al. 2008).

In general, laboratory-based measurements are made over fairly small samples, and spectroradiometers are used to obtain spectral data. Laboratory-based data

acquisition has the advantage of providing controlled conditions and the highest quality reflectance, but it also requires the transport of surfaces to the laboratory; in many cases, this transport is infeasible. For field measurements, a number of field spectroradiometers are available (e.g., FieldSpec, Spectron- SE590, ASD Personal Spectrometer II). Airborne multi- and hyperspectral scanners, such as the Airborne Visible/Infrared Imaging Spectrometer (AVIRIS), HyMap or Compact Airborne Spectrographic Imager, have been used to acquire spectral data (Milton, Fox, and Schaepman 2006; Roberts and Herold 2004). For acquired spectral data, most sensors are mounted vertically over the target (nadir view). The same instrument is used to measure the energy (in terms of digital-number (DN) pixel values that have not yet been calibrated into physically meaningful units) of both the material and the reference panel (Roberts and Herold 2004), which is a nearly ideal Lambertian reflecting surface with known high reflectance (near 1) and spectrally flat. A conversion of the DN to radiance values can be performed through the calibration process using data from the sensor manufacturing company. Afterwards, a ratio between radiances for the target and the reference yields reflectivity values. Alternatively, reflectivity (the real intrinsic characteristic of a material) can be calculated through a simple ratio between the DN value corresponding to the target and the radiometric reference. However, the manufacturer calibration process takes into account more subtle variations, for example, the spectral alignment (Markelin et al. 2008).

Table 1 shows some of the existing spectral libraries of urban materials. These libraries provide information on impervious and pervious materials and from the VIS, NIR, SWIR, and TIR spectral ranges.

Table 1. Spectral libraries of impervious and pervious materials based on Kotthaus et al. (2014).

References	Country	Urban surface cover type		Roof material	Spectral range (nm)	Instrument	Data acquisition		
		P	I				L	F	A
Baldrige et al. (2009) ASTER	USA	•	•	Metals, rubber, asphalt, tile, roofing paper, shingle	400-1000 1000-2400 8000-12000 VIS-NIR-SWIR TIR	Advanced Spaceborne Thermal Emission Reflection Radiometer	•	•	
Herold et al. (2004) Santa Barbara spectral library	USA	•	•	Wood, shingle, tile, gravel, asphalt, roofing paper	350–2400 VIS-NIR-SWIR	ASD FieldSpec 3 Spectroradiometer AVIRIS		•	
Heiden et al. (2007)	Germany	•	•	Mineral, metallic, hydrocarbons Tile, fibre cement, steel, aluminium, concrete, polyethylene, polyvinyl chloride, painted roof	400–2500 VIS-NIR-SWIR	HyMap HRS & ASD FieldSpec 3 Spectroradiometer		•	•
Moreira and Galvão (2010)	Brazil		•	Asbestos, concrete, metal deck, polycarbonate, clay tile, zinc	400-2400 VIS-NIR-SWIR	ASD FieldSpec 3 Spectroradiometer	•	•	
Nasarudin and Shafri (2011) UPMSpeclib	Malaysia	•	•	Tile, shingle, metal, polyvinyl chloride, concrete	350-2500 VIS-NIR-SWIR	ASD FieldSpec 3 Spectroradiometer		•	
Kotthaus et al. (2014) SLUM	England		•		350-2500 2000-15400 VIS-NIR-SWIR-TIR	HR-1024 Spectroradiometer M2000 Fourier Transform Infrared spectrometer	•		

The urban surface cover type includes some (P) pervious and (I) impervious roof materials. The spectral data were obtained in the laboratory (L), the *field* (F) or from an airborne (A) sensor. ASD: analytical spectral devices. HRS: hyperspectral remote sensing. ASTER: Advanced Spaceborne Thermal Emission Reflection Radiometer. The ASTER library includes contributions from the Jet Propulsion Laboratory (JPL), Johns Hopkins University (JHU) and the United States Geological Survey (USGS).

Even with the existing libraries, information is still needed on commonly used roof materials according to different geographic regions. Furthermore, new building materials such as plastics and metals continuously enter the market, and their spectral characteristics have limited presence in the existing spectral libraries (Heiden et al.

2007; Kotthaus et al. 2014; Jilge et al. 2017).

In this regard, this work aims to contribute to the knowledge of the spectral characteristics of roof materials. The main perspective is the future use of spectral data for roof classification, allowing the assessment of roofs for implementing FWE systems. The objectives of this work are 1) to describe a methodology for spectral data acquisition of common roof materials from the Mediterranean region and 2) to develop a spectral library of common roof materials in urban areas.

2. Materials and methods

2.1. Roof materials

Common roof materials in urban areas, including some representative materials from the Mediterranean region, were selected according to the literature (Castellanos 1996; Chueca 2003; Schunck et al. 2003; Farreny et al. 2011; Nadal et al. 2017). In total, 39 samples were collected. All the samples were in new condition. Granite, slate and wood roofs were also included, as they are common on rooftop open terraces. Various colours were considered in the selection. Each sample was coded with a letter identifying the material class and an ID number. Table 2 describes the characteristics of the roof material samples used in this study: ceramics (5), fibre cement (1), concrete (3), metals (9), paints (2), plastics (11), stone (7), and wood (1).

Table 2. Characteristics of the roof material samples used to acquire the spectral data.

ID	Class	Material	Colour	Dimensions (mm)
C01	Ceramic	Ceramic tiles	Burnt red, dull	400 × 400 × 20
C02	Ceramic	Gres porcelain tiles	White, shiny	300 × 600 × 6
C03	Ceramic	Gres porcelain tiles	Red	300 × 600 × 6
C04	Ceramic	Gres porcelain tiles	Grey, dull	410 × 410 × 5
C05	Ceramic	Gres porcelain tiles	Multicoloured burnt	315 × 315 × 5

ID	Class	Material	Colour	Dimensions (mm)
			red/brown/dark green, dull	
T01	Concrete	Concrete tiles	Grey, dull	200 × 200 × 40
T02	Concrete	Concrete tiles	Grey, dull	400 × 400 × 35
T03	Concrete	Concrete bricks	Grey, dull	95 × 200 × 75
T04	Cement	Corrugated fibre cement shingles	Grey, dull	300 × 300 × 3
M01	Metal	Steel shingles	Grey, dull	250 × 500 × 0.06
M02	Metal	Galvanized steel shingles	Grey, shiny	250 × 500 × 0.05
M03	Metal	Inox steel shingles	Grey, shiny	250 × 500 × 0.05
M04	Metal	Aluminium shingles	Grey (polished)	250 × 500 × 1
M05	Metal	Steel shingles with paint	Beige	400 × 300 × 0.05
M06	Metal	Copper shingles	Copper	250 × 500 × 0.05
M07	Metal	Zinc shingles	Grey	250 × 500 × 0.06
M08	Metal	Steel with paint (sandwich panels)	Beige	400 × 300 × 35
M09	Metal	Aluminium with paint (sandwich panels)	Grey, dull	270 × 185 × 50
PT01	Paint	Shingles with paint	Blue, synthetic enamel	300 × 300 × 10
PT02	Paint	Shingles with paint	Red, synthetic enamel	300 × 300 × 10
P01	Plastic	Methacrylate shingles	Blue, shiny	300 × 250 × 3
P02	Plastic	Methacrylate shingles	Red, shiny	300 × 250 × 3
P03	Plastic	Methacrylate shingles	White, shiny	300 × 250 × 3
P04	Plastic	Polyvinyl chloride (PVC) shingles	White	500 × 250 × 3
P05	Plastic	Polycarbonate shingles	White, shiny	190 × 150 × 1
P06	Plastic	Polycarbonate shingles	Translucent blue, shiny	190 × 140 × 1
P07	Plastic	Polycarbonate shingles	Translucent shiny	210 × 297 × 8
P08	Plastic	Polycarbonate shingles	Translucent blue, shiny	210 × 297 × 8

ID	Class	Material	Colour	Dimensions (mm)
P09	Plastic	Polycarbonate shingles	Translucent red, shiny	210 × 297 × 8
P10	Plastic	Synthetic rubber ethylene–propylene– diene monomer rubber	Black, dull	210 × 310 × 1
P11	Plastic	Asphalt polymer	Black, dull	300 × 300 × 1
S01	Stone	Granite tiles	Multicoloured White/black, dull	150 × 150 × 20
S02	Stone	Granite tiles	Multicoloured Black/grey/white, dull	150 × 150 × 20
S03	Stone	Granite tiles	Multicoloured White/green, dull	150 × 150 × 20
S04	Stone	Granite tiles	Multicoloured White/pink/black, dull	150 × 150 × 20
S05	Stone	Slate tiles	Grey, dull	300 × 600 × 10
S06	Stone	Gravel	Multicoloured grey/beige, dull	400 × 300 × 15
S07	Stone	Gravel	Multicoloured grey/white/beige, dull	400 × 300 × 15
W01	Wood	Wood shingles	Light brown, dull	300 × 300 × 10

2.2. Equipment and software

The Airborne Imaging System for different Applications (AISA) Eagle II sensor was used to acquire the spectral data (Alamús et al. 2018).

Table 3 describes the technical parameters of the airborne sensor. The AISA sensor, manufactured by Specim, is a commercial pushbroom-type imaging spectrometer system that records the VIS-NIR spectral range. It has a reflection grating with a two-dimensional solid-state array detector based on charge-coupled devices (CCD) (Alamús et al. 2018).

Table 3. Technical parameters of the AISA Eagle II imager.

Parameter	AISA Eagle II
Field of view (FOV)	37.7°
Spectral bands	252
Spectral range	400-1000 nm
Spectral resolution	2.5 nm
Across-track spatial pixels	1024 pixels
Swath width	47 cm

To obtain homogeneous samples, a specific system was designed. It consisted of a workbench on which the sensor was installed, remaining fixed during data acquisition. A standard Mecalux® bench was used for this purpose. Below the sensor, a linear unit was installed. The linear unit allows movement of the sample and the Spectralon® (radiometric reference) under the sensor at a constant speed. Figure 1. shows the linear unit built for this work. The linear unit was equipped with a rail and a rolling platform driven by a stepper motor, plus a servo control that allows the selection of software parameters for driver movement, including the path and the speed of the platform. The speed was computer controlled using Ezi-MOTION Plus-R manufactured by direct 2 motion.



Figure 1. Linear unit built for displaying the roof material samples and the Spectralon® panel.
View of the rail (left) and the linear unit platform and motor system (right).

A Spectralon® reflectance reference panel manufactured by Labsphere was used during spectral acquisition. Figure 2. Illumination geometry for data acquisition in the laboratory. shows the light sources designed to provide sufficient energy in the spectral domain captured by the AISA Eagle II sensor. Two light sources were used to illuminate the sample, which gave a more spectrally homogeneous field of irradiance than that from a single source. For this purpose, two different lamps were used, and they illuminated the scene parallel to the slit opening of the sensor to avoid specular reflections: a 50 W LED lamp emitter with higher intensity emittance in the green-blue VIS spectral ranges and a standard 500 W halogen lamp, characterized by a peak in the yellow to near-infrared range. Figure 3 shows the emission spectrum of the lamps measured in the laboratory. The use of the LED together with the halogen lamp has the objective of obtaining the maximum illumination in the entire VIS-NIR spectral range to optimize the signal-to-noise ratio in the process of data acquisition.

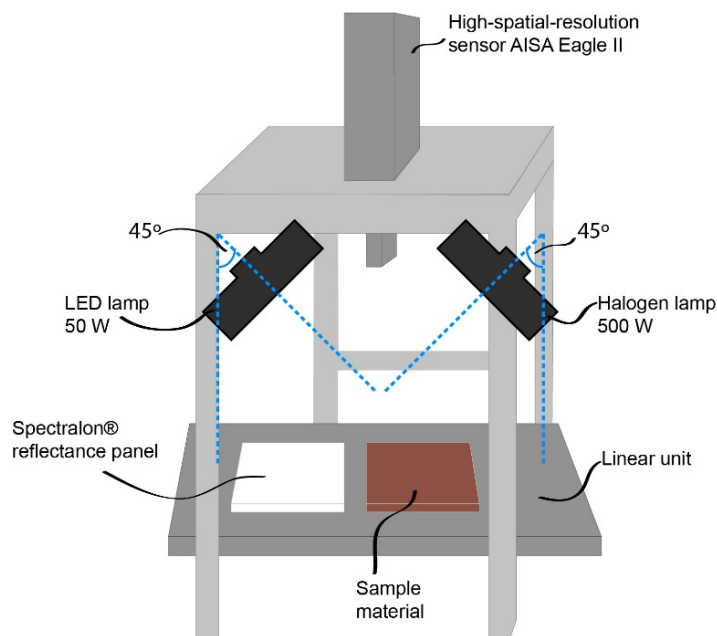


Figure 2. Illumination geometry for data acquisition in the laboratory.

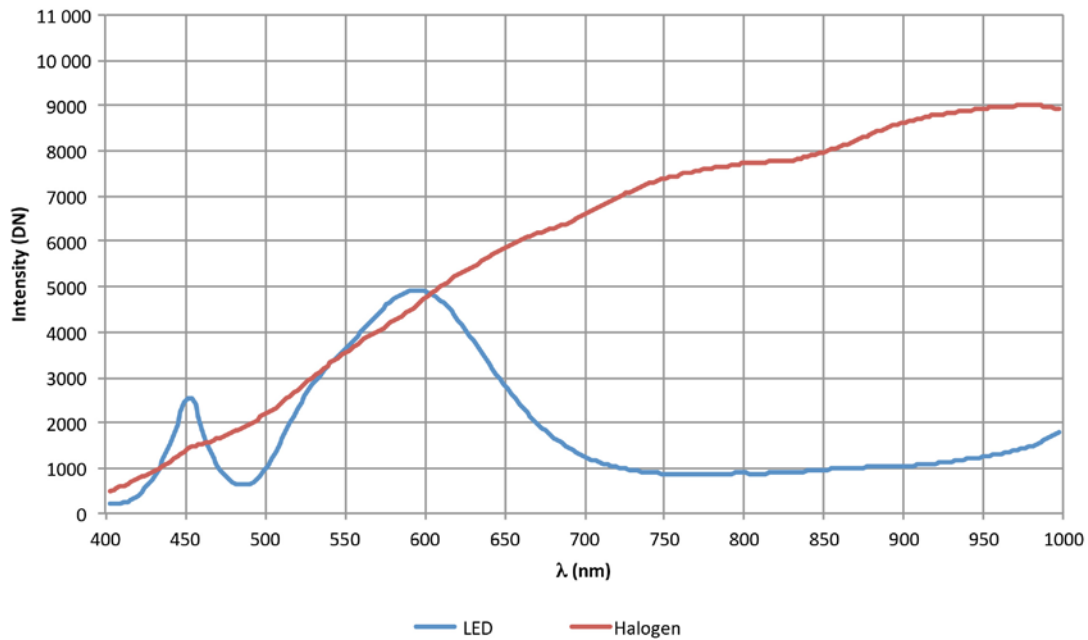


Figure 3. Emission spectrums of the LED and halogen lamps used for data acquisition in the laboratory.

The essential software used in this study includes GeoView 2, which specializes in the management of raster and vector layers developed for internal use by the Cartographic and Geologic Institute of Catalonia (ICGC), and a script (see the appendices).

2.3. Procedure

Figure 4 shows the four main processing stages of the described methodology: spectral data acquisition, image preprocessing, radiance data processing, and the development of the spectral library. A detailed description of each stage is presented in the following sections.

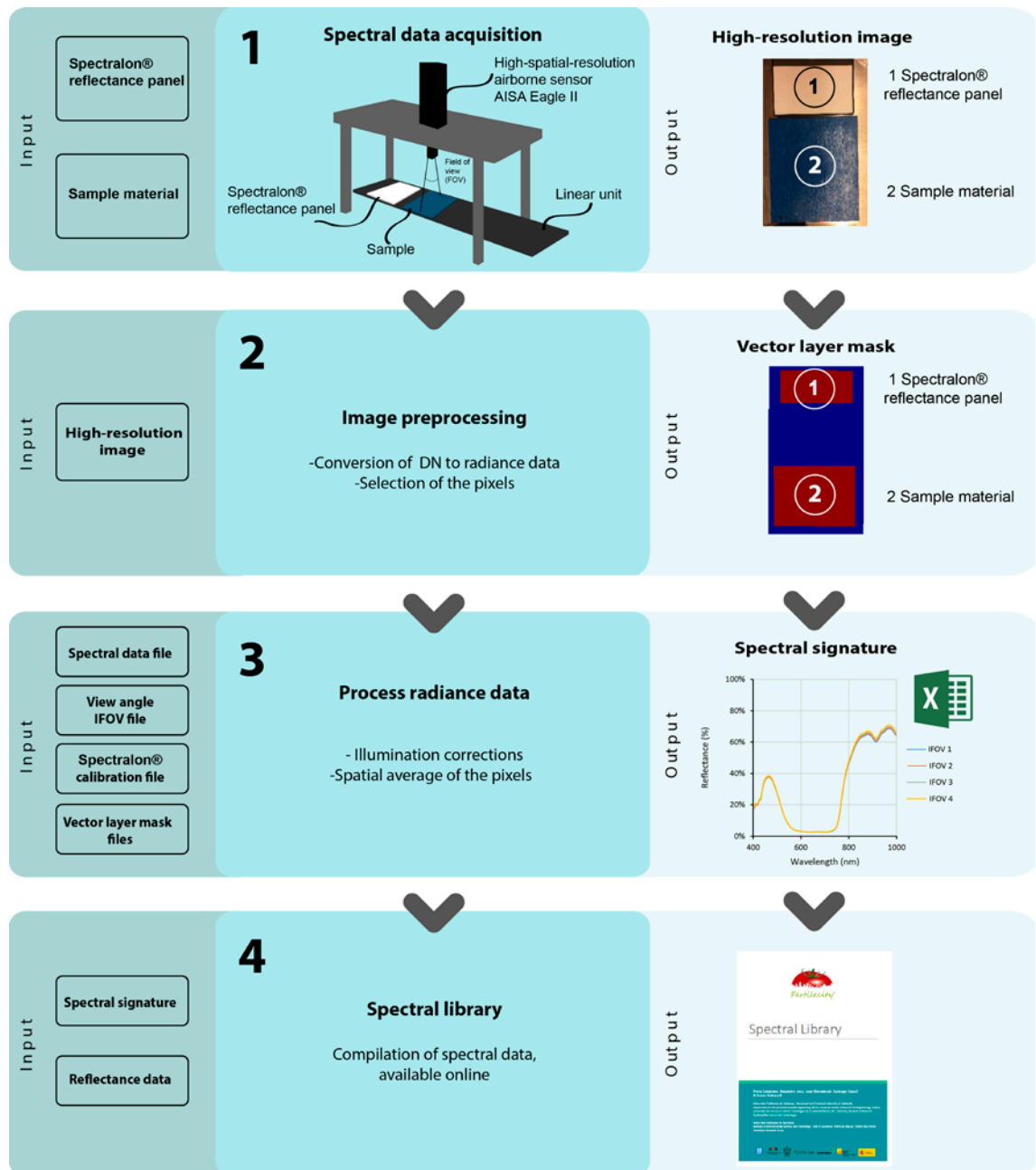


Figure 4. Diagram of the framework for laboratory-based spectral data acquisition of roof materials and the development of the spectral library.

2.3.1. Spectral data acquisition

Spectral data acquisition was performed in the Hyperspectral Laboratory of the ICGC under controlled conditions. The laboratory was isolated from natural light as well as artificial light sources from adjacent spaces. Artificial lights described in the previous section were used to illuminate the sample materials and to ensure uniform illumination.

Radiance data were captured in the VIS-NIR spectral region from samples of common roof materials (identified in the literature) with the AISA Eagle II sensor. The spectral data were acquired by sampling each material together with the reflectance reference panel. Both of these objects were placed on the linear unit (Figure 5), and the sensor was placed in the nadir angle position (along-track viewing position).

To obtain a similar pixel size for the along and across tracks, speed tests were performed before data acquisition. The speed at which a pixel was as square as possible was 4 mm s^{-1} . The pixel resolution width and length were 0.45 mm and 0.40 mm, respectively. The average time needed for the data collection process for each material was 4 minutes. Each data acquisition instance was registered on paper, with three main information items: general data (date, sample ID, start and end time, consecutive number of data tests acquired); laboratory conditions (operation and conditions of the lighting and linear unit); and incident reports.



Figure 5. Top view of the Spectralon ®, sample material (in this case, ceramic tile C01), and linear unit platform for spectral data acquisition.

2.3.2. Image data preprocessing

VIS-NIR spectral radiance data were obtained using the AISA Eagle II sensor that records high-spatial-resolution images and spectra in raw DN. To obtain the radiance,

DNs were converted to radiance values using a calibration process. This process was performed through a proprietary calibration protocol from the sensor manufacturing company. The images were composed of the reflectance reference target, the sample material and the linear unit. To process the radiance data, valid pixels were selected from each image recorded, and two vector masks were made: the first mask was from the Spectralon® panel, and the second mask was from the roof material. This process was performed with GeoView 2.

2.3.3. Processing the radiance data

The pixel array was divided into four groups corresponding to different instantaneous fields of view (IFOVs). As Figure 6 illustrates, the four groups were $-3^{\circ}:0^{\circ}$ & $0^{\circ}:3^{\circ}$; $-7^{\circ}:-3^{\circ}$ & $3^{\circ}:7^{\circ}$; $-12^{\circ}:-8^{\circ}$ & $8^{\circ}:12^{\circ}$; and $-17^{\circ}:-13^{\circ}$ & $13^{\circ}:17^{\circ}$. These view angles were set in a script (available in the Appendices) to process the raw data in the different IFOVs.

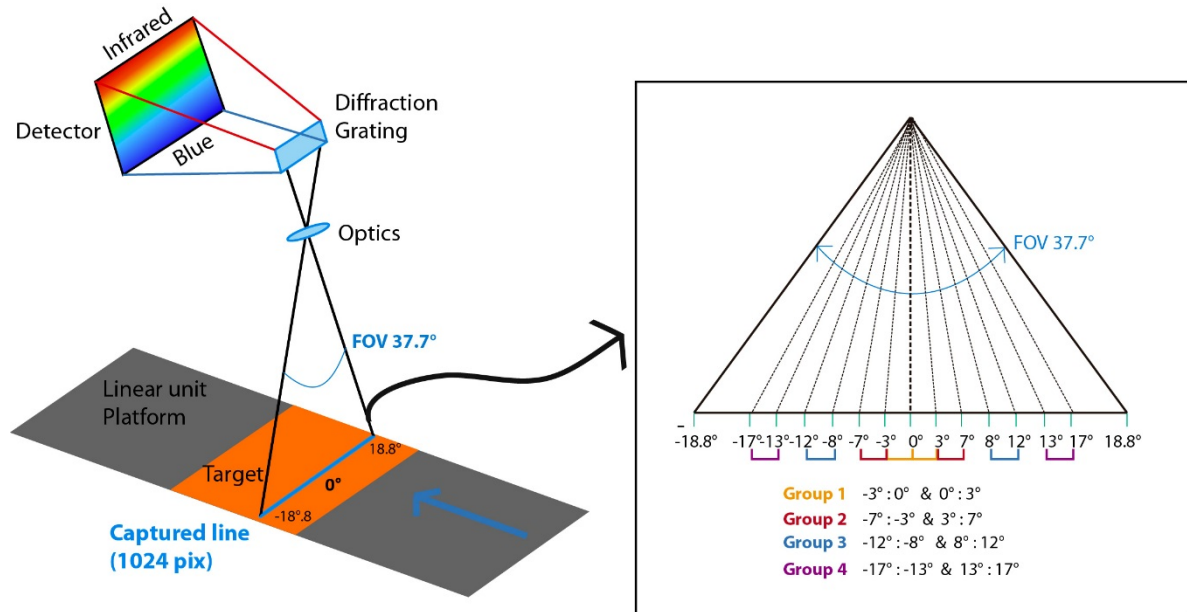


Figure 6. IFOV groups.

The corresponding angular mask was obtained for each IFOV group. An overlap of two (i.e., the sample material and the reference target) three-dimensional arrays was made. The pixels of the sample material and the reflectance panel were spatially and

temporally averaged. Illumination corrections were performed using the calibration file provided by the Spectralon® manufacturer.

Reflectance data were obtained for each IFOV group using Equation (1). The absolute spectral reflectance α_λ was calculated by dividing the sample material radiance $Rad_{\lambda sample}$ by the reflectance panel (Spectralon®) $Rad_{\lambda reference}$ and by including the spectral reflectance of the Spectralon® Ref_λ .

$$\alpha_\lambda = \left(\frac{Rad_{\lambda sample}}{Rad_{\lambda reference}} \right) Ref_\lambda \quad (1)$$

Figure 7 shows an example of the output script, which is composed of a series of five images and a file with the reflectance data for each roof material and view angle group. Images a through e contain a full-scene image (i); a sample mask (ii); a reference panel mask (iii); a view angle mask (iv); an image of the overlap between the view angle mask and the material mask (v); and an image of the overlap between the angle mask and the reference panel mask (vi). The fifth image corresponds to the spectral signatures of the four view angle groups.

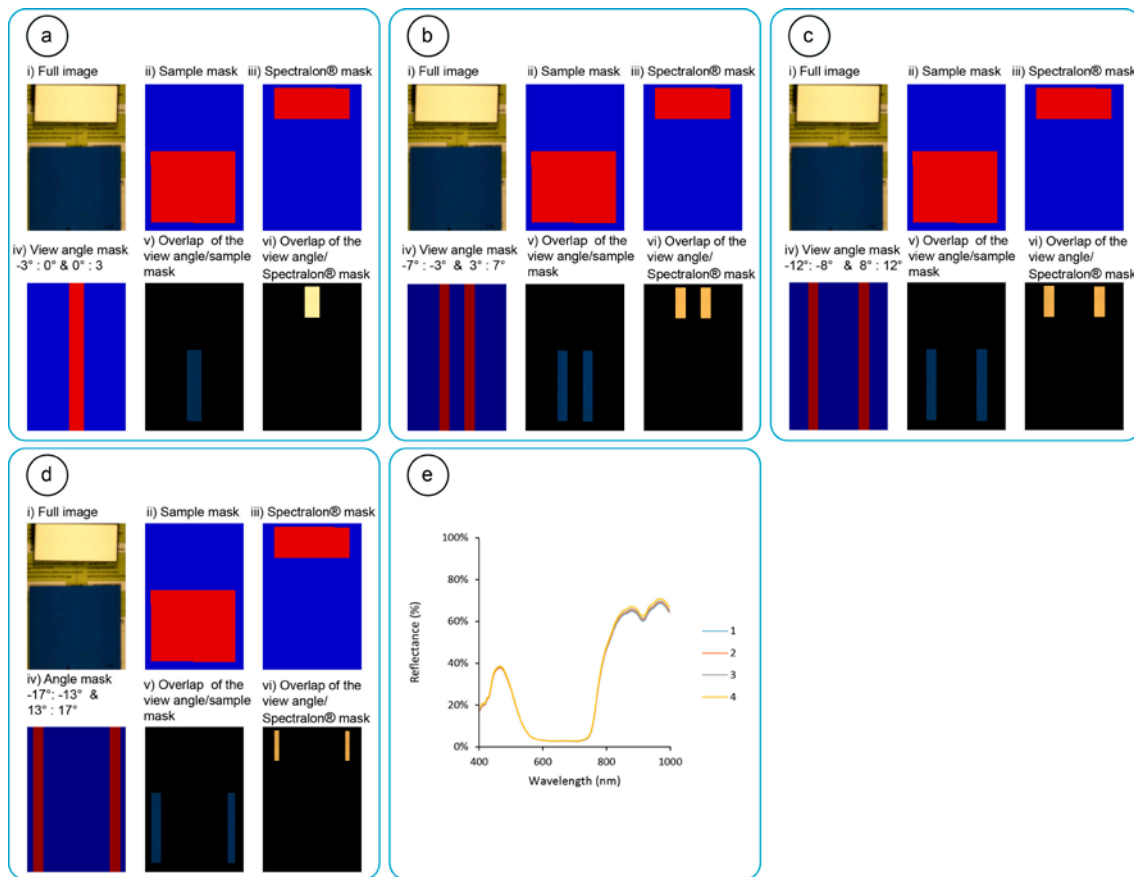


Figure 7. Example of a series of five (a through e) images output of the script, in this case shingles with blue paint (PT01).

The available number of pixels to obtain the spectral reflectance data and create the spectral signatures were in the following ranges: 38,033 to 162,928 for IFOV 1; 50,997 to 218,300 for IFOV 2; 12,214 to 223,523 for IFOV 3 and from 0 to 223,893 for IFOV 4. The available number of pixels of each sample material and IFOV group are shown in the Appendices.

2.4. Spectral library

All the acquired spectral reflectance data were compiled into a file.

2.5. Spectral separability

After the compilation of the spectral reflectance data (spectral library), a spectral separability analysis was performed. The approach to spectral separability was

calculated using (the root mean square (RMS)) Equation (2), considering reflectance data in the VIS-NIR (400 to 1000 nm) spectral range and the four IFOV groups. A selection of 36 materials within and between classes was made. This selection was conducted randomly, considering similar and different reflectance data and considering the representative materials from the Mediterranean region.

$$RMS = 1/N \sqrt{\sum_{i=1}^N (A_i - B_i)^2} \quad (2)$$

3. Results

In total, 52 laboratory tests were carried out, including pilot tests. VIS-NIR reflectance data of all (39) roof sample materials and the four view angle groups were obtained. However, in 10 (from P05 to P09, from S01 to S04 and T03) cases, it was not possible to obtain data from the fourth view angle group due to the small size of the sample material.

3.1 Spectral signatures by material class

In this section, the spectral reflectance of view angle group 1 for all the materials analysed is presented by material class. The results of the remaining three view angle groups are available in the spectral library.

3.1.1. Ceramics

Figure 8 shows the VIS-NIR spectral signatures of the ceramic samples. White ceramic (C02) showed a high and constant reflectance, with values ranging from 84% to 88%, due to its uniformly light colour and bright surface. Red ceramics (C01, C03, and C05) revealed a deep absorption reflectance between 420 nm and 5500 nm. Slight absorption was observed at approximately 650-700 nm and increased by 60% (to 900 nm). Grey

ceramic (C04) demonstrated constant reflectance and slight absorption at approximately 600-700 nm.

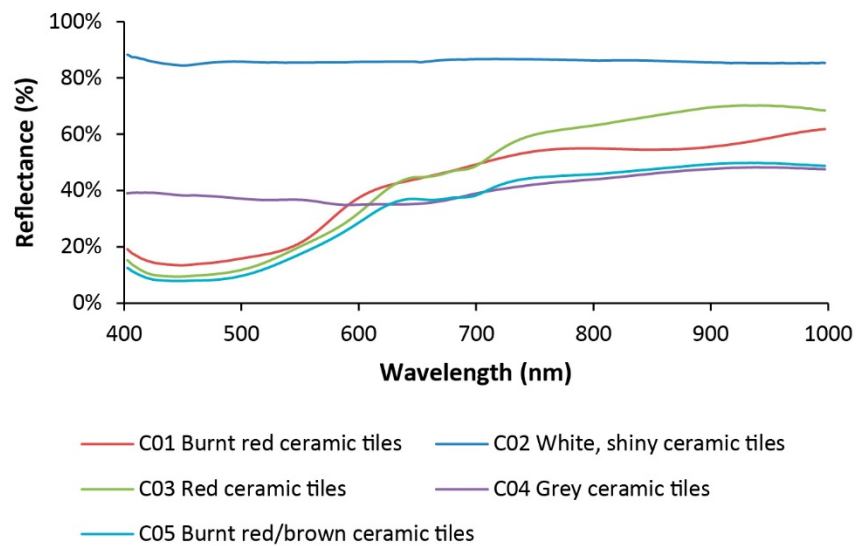


Figure 8. Spectral reflectance of ceramics.

3.1.2. Fibre cement and concrete

Compared with other material classes, the fibre cement and concrete spectral signatures (Figure 9) demonstrated minor differences within them. The reflectance values of most of these material classes (T01, T02 and T03) increased slightly at approximately 550-600 nm and increased up to approximately 600 nm. The fibre cement sample (T04) exhibited the lowest and most constant reflectance values of the samples in this category. The materials presented low reflectance values from 17% to 33%.

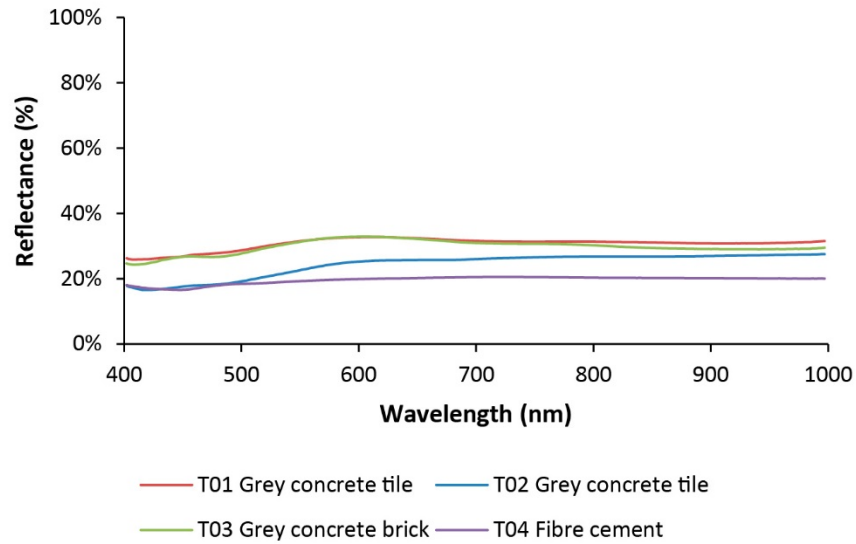


Figure 9. Spectral reflectance of fibre cement and concrete.

3.1.3. Metals

The VIS-NIR reflectance of the metal samples is represented in Figure 10. Most of the metals exhibited values ranging between 12% and 30% and constant reflectance values between 600 nm and 997 nm. Almost all the metal samples (except for M05) demonstrated a slight increase at approximately 400-470 nm, and a slight absorption was observed at approximately 470-500 nm. Some of the steels (M05 and M08) demonstrated the highest reflectance values (from 58% to 80%). Polished aluminium and zinc (M04 and M07) showed the lowest reflectance values (4%-11%).

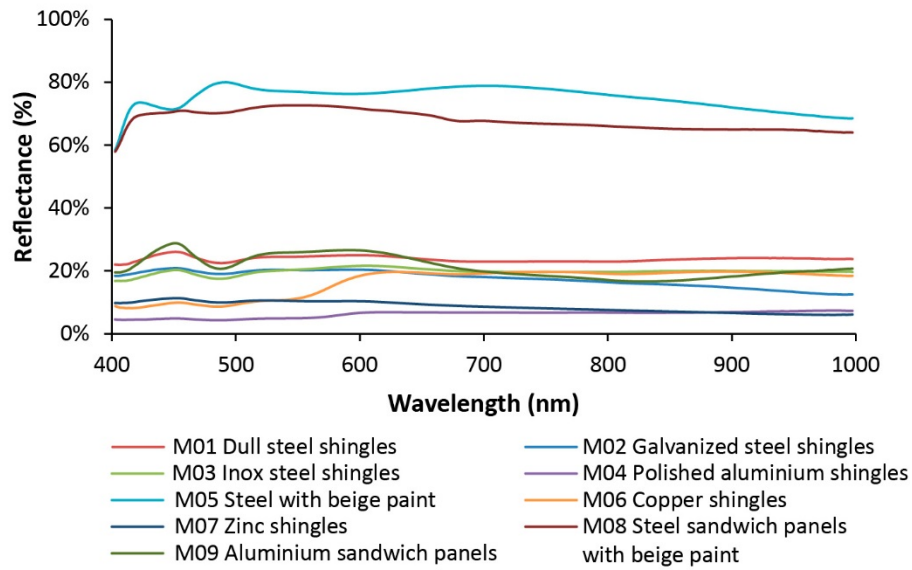


Figure 10. Spectral reflectance of metals.

3.1.4. Paints

The VIS-NIR spectra of paints (Figure 11) showed pronounced increases and absorption peaks. PT01 had its highest reflectance peak (69%) at approximately 960 nm and the lowest reflectance peak (3%) between 600 nm and 740 nm. PT02 demonstrated the lowest reflectance (3%) at approximately 450-550 nm and its highest peak (74%) at approximately 960-997 nm.

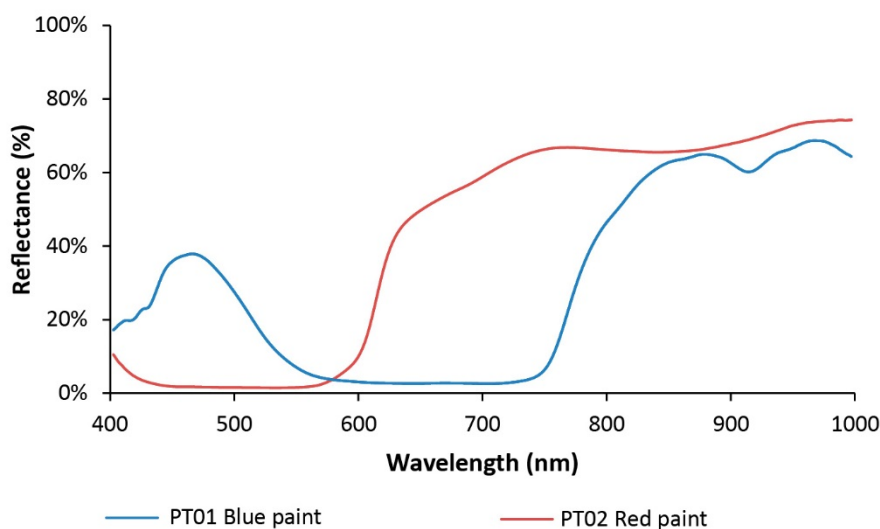


Figure 11. Spectral reflectance of paints.

3.1.5. Plastics

The VIS-NIR reflectance of plastic samples (Figure 12) exhibited great variability in the spectral shapes. White plastics (P03 and P04) had similar values, ranging from 64% to 88%, which were the highest among all the plastic samples. P03 presented a slight increase. PVC (P04) exhibited more constant values (between 736 nm and 997 nm); this outcome was in contrast to white methacrylate (P03), which demonstrated a decrease at approximately 800 nm and a slight increase at approximately 930 nm. Plastics P01, P03, P04, P05, P06, P07 and P08 revealed three crests in their spectral shapes: large increases at approximately 410-468 nm and large decreases at approximately 511-700. P02 and P09 exhibited two peaks, with a large decrease at approximately 418-588 nm and a large increase at approximately 590-800 nm. P10 and P11 showed very similar spectral shapes and constant reflectance values between 3% and 6%.

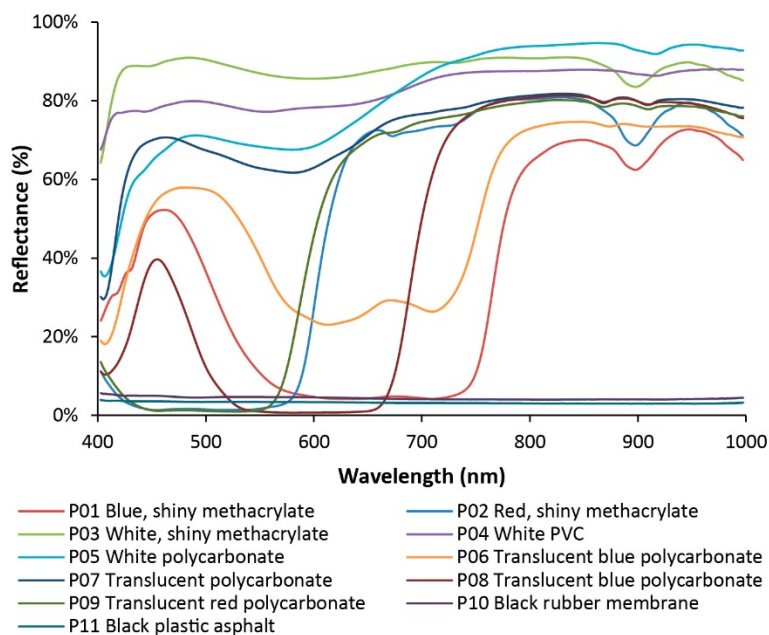


Figure 12. Spectral reflectance of plastics.

3.1.6. Stones

Granite samples (S01, S02, S03 and S04) showed a slight increase in reflectance at 500-600 nm. The granite samples presented reflectance values from 39% to 50%, except for S2, with low values ranging from 24% to 30%. All samples presented low variability in reflectance. The slate sample (S05) revealed the lowest reflectance, ranging from 19% to 25%, and its spectral shape was the same as that of the granite samples. Gravel, slate and dark granite samples presented the lowest reflectance values. Gravel samples showed absorption between 410 nm and 495 nm and a slight reflectance peak between 500 nm and 565 nm; the reflectance values ranged from 18% to 28% (Figure 13).

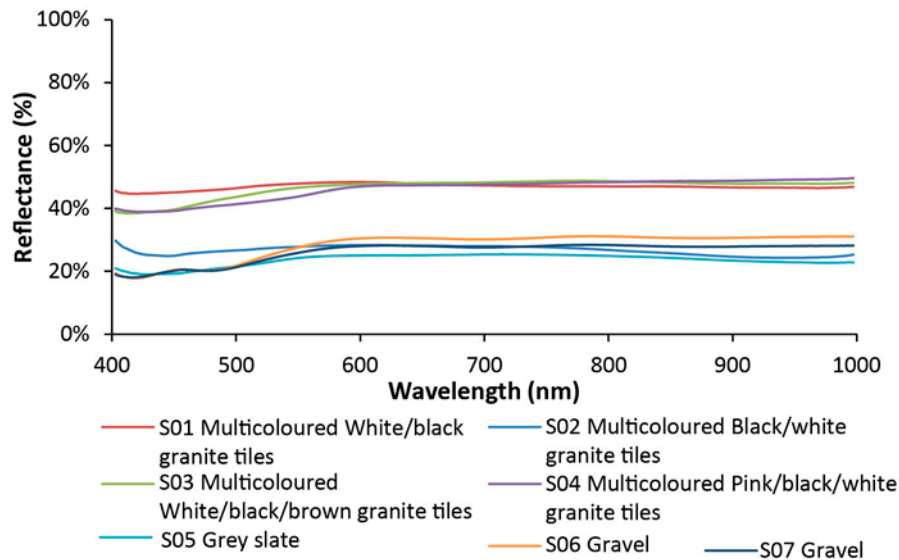


Figure 13. Spectral reflectance of stones.

3.1.7. Wood

Figure 14 illustrates the spectral signature of the wood sample. W01 showed a low reflectance (26%) at approximately 400-500 nm and a high reflectance peak (82%) up to approximately 800-942 nm.

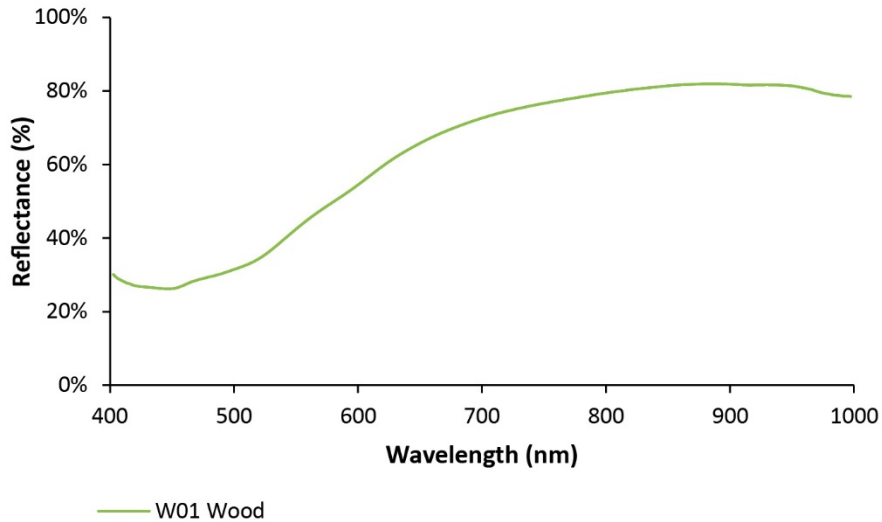


Figure 14. Spectral reflectance of wood.

3.2. Representative roof materials from the Mediterranean region

In this section, the spectral reflectance of only view angle group 1 is presented first, and then all the view angle groups are presented. Figure 15 shows a selection of 6 representative roof materials from the Mediterranean region (Nadal et al. 2017; Farreny et al. 2011; Zinzi 2010).

The results showed different spectral shapes and reflectance values according to the material. Fibre cement (T04), grey concrete (T02) and gravel (S07) showed a flat spectral shape and the lowest reflectance (from 17% to 28%) compared with that of the other materials. Red ceramic (C01) showed reflectance values from 13% (403 nm) to 62% (approximately 997 nm), and the higher reflectance was in the NIR spectra. Polycarbonate (P05) exhibited the most variability in the spectral shape, and reflectance values from 35% (407 nm) to 95% (845-879 nm) were identified. The steel sandwich panel (M08) presented slight differences in the reflectance values, from 58% (403 nm) to 73% (532-569 nm).

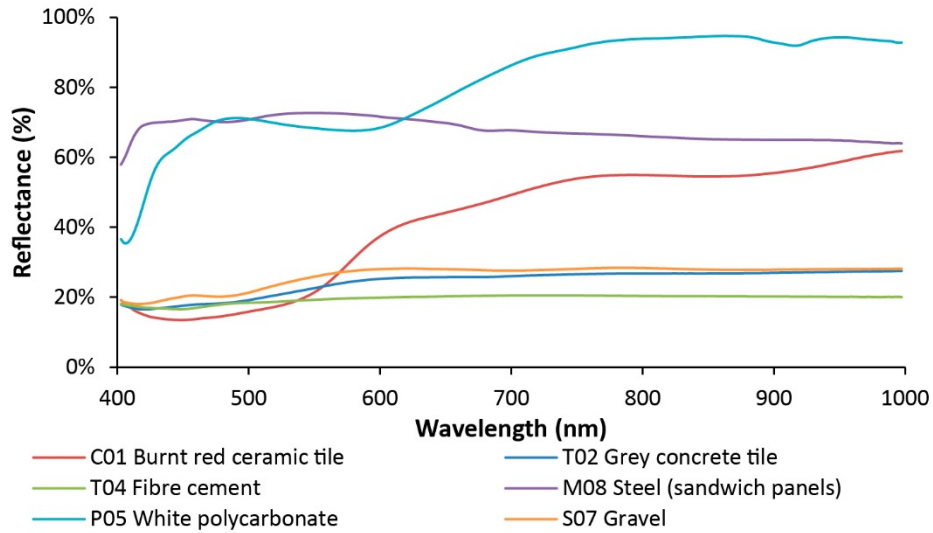


Figure 15. Spectral reflectance of the representative roof materials in the Mediterranean region.

Figure 16 illustrates the spectral signatures of the representative Mediterranean roof materials of the four IFOV groups. The materials presented the same spectral signatures compared within the IFOV groups of each material. The polycarbonate (P05) exhibited some larger differences in the amplitude of the reflectance signature; however, the spectral shape remained unchanged.

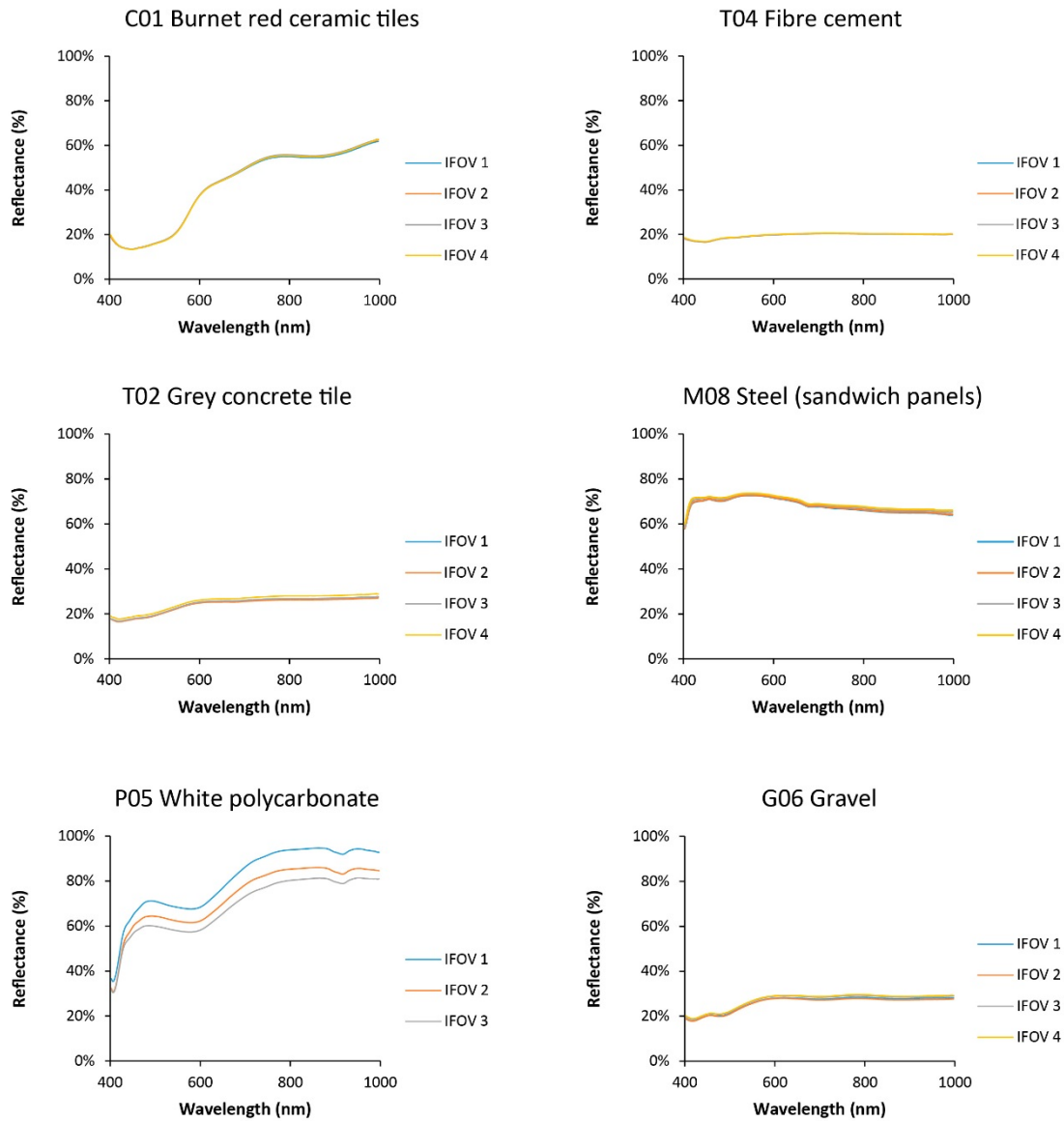


Figure 16. Spectral reflectance of the representative roof materials of the Mediterranean region and the four IFOV groups.

3.3. Spectral library

The spectral library is divided into seven sections. It includes specific information about each sample material, photographs, and spectral signatures. A file with the reflectance values from each material is also provided. The spectral library of rooftop materials in the urban area (Zambrano-Prado et al. 2017) can be acquired free online at <https://ddd.uab.cat/record/196065>

3.4. Spectral separability of roof materials

Figure 17 shows the results of a quantitative analysis of spectral separability. A comparison among 36 materials was made. The average score of separability was 3.43. A score of 0 means that there is no separability, while a score increase indicates greater separability among the roof materials.

Ceramic materials, burnt red (C01) and white (C02) ceramic tiles, showed a spectral separability of 10.61. In the case of ceramics (C01 and C05) with similar red colours, a low separability of 1.34 was found. Separability results between red ceramic tile (C01) and fibre cement (T04) showed a score of 4.32. Regarding metal materials, a low spectral separability score of 1.77 between M03 and M07 was found, while the separability comparison between M04 and M08 was higher (9.94). The steel sandwich panel (M08) and white plastic (P05) showed a value of 2.66. Regarding plastic materials, a score separability value of 4.01 was found between blue (P01) and translucent blue (P08). A low value of 1.08 was found between plastics (P03 and P04) with a similar white colour. The highest separability score (13.38) was found between white (P03) and black (P10) plastics. The results showed a low value (0.19) between black plastics (P10 and P11). Paint surfaces (PT01 and PT02) showed a separability score of 4.88. With respect to the stone materials class, a low separability of 0.49 was found within multicoloured granite tiles (S01 and S04). The results showed a separability score of 3.12 between multicoloured granite tiles (S01) and gravel (S06). Low separability of 0.24 was found for two types of gravel (S06 and S07). The results between gravel (S07) and concrete (T02) showed low (0.35) spectral separability. The lowest separability (0.15) was found between the concrete tile and brick (T01 and T03), and a value of 1.35 was found within two concrete tiles (T01 and T02). Finally, a

spectral separability of 1.83 was found between the concrete tile (T01) and ceramic tile (C04).

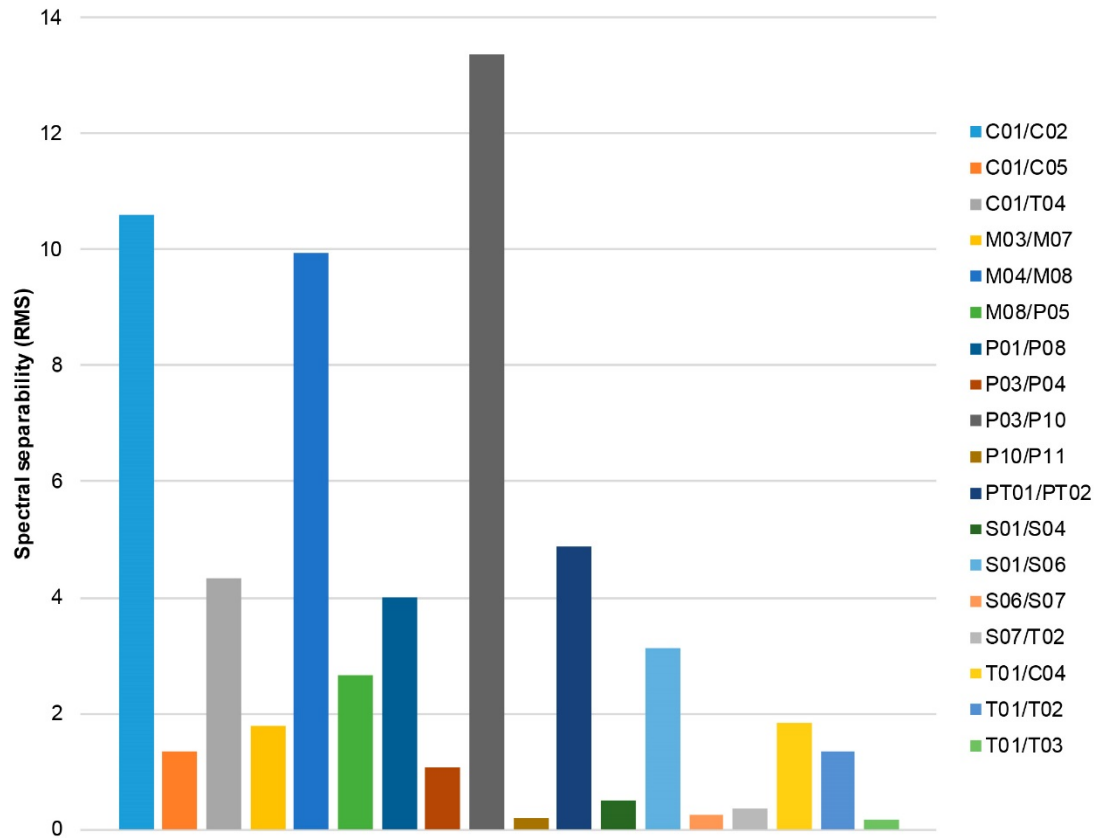


Figure 17. Spectral separability average scores for roof materials.

4. Discussion

The ceramic (C01, C03, C05) spectra varied greatly, and a strong absorption for red ceramics occurred in the visible region from 420 to 550 nm. These results confirm the existence of iron oxide features normally present in ceramic materials. These results agree with those found by Nasarudin and Shafri (2011) for clay tiles (strong absorption near 550 nm).

The spectra of the fibre cement and concrete class showed a reflectance increase up to approximately 600 nm, which could indicate the presence of silica and carbonates

in both materials. A clear difference in the spectral characteristics between fibre cement and concrete was not identified. The reflectance signatures of these materials were flat and low due to their dark grey surface coating. These results are similar to those obtained by Nasarudin and Shafri (2011) and Kotthaus et al. (2014).

All metal materials showed similar spectral shapes, increasing reflectance peaks at approximately 450 nm and absorption reflectance peaks at 500 nm, and most of them showed low reflectance values, especially in the NIR reflectance. Some painted samples (M05 and M08) were included in the metal category, and these materials (M05 and M08) showed the highest reflectance due to the influence of the paint colour. Nasarudin and Shafri (2011) and Kotthaus et al. (2014) found similar spectral characteristics for the similar metal materials analysed in this work.

The plastic samples showed great variability depending on the colour in terms of reflectance for visible wavelengths. The reflectance signatures of P10 and P11 were characterized by low reflectance throughout the whole VIS-NIR region due the dark colour of the samples. The NIR reflectance showed the same deep absorption (at approximately 900 nm) for all samples with the exception of the translucent plastics; these samples showed a slight absorption for the NIR wavelengths. The two absorption reflectance peaks (600 and 901 nm) for P01, P03 and P05 were similar to those (PVC sheets) obtained by Kotthaus et al. (2014).

The reflectance spectra of stones vary slightly. These samples reveal two differentiated groups: 1) from S01 to S05 and 2) S06 and S07. Group one showed similar absorption bands (from 420 to 500 nm). Group two (gravels) showed two absorptions (423 and 486 nm) and increasing peaks (452 and 576 nm). The S01, S02, and S03 samples have a higher overall reflectance due to the presence of mostly light

colours in the multicoloured samples. Kotthaus et al. (2014) found similar reflectance spectra (absorption bands from 350 to 500 nm) for multicoloured granite.

In the case of paint samples, variability was observed for visible wavelengths depending on the colour. The NIR reflectance showed an absorption at approximately 900 nm. The spectral reflectance of the paint sample was somewhat comparable to the signature of the plastic samples due to the similar component materials.

It was confirmed that the IFOV modifies the overall amplitude of the reflectance signature but not the spectral signatures (Hapke 2012).

The development of a spectral library provides knowledge on the spectral characteristics of common roof materials, not only some that can be found in the Mediterranean region but also new building materials such as metals and plastics that are still underrepresented in existing spectral libraries (Jilge et al. 2017; Kotthaus et al. 2014).

Low spectral separability was found within materials from the following classes: red ceramics (C01 and C05) 1.34; dark metals (M03 and M07) 1.77; black plastics (P10 and P11) 0.19; white plastics (P03 and P04) 1.08; granite tiles (S01 and S04) 0.49; gravels (S06 and S07) 0.24; and grey concrete tiles (T01 and T02) 1.35.

Additionally, low spectral separability between the following different material classes was found: grey concrete tile and grey ceramic 0.35; grey concrete and gravel 1.83; red ceramic and fibre cement 4.32; and steel sandwich panel and white plastic 2.66. In contrast, higher spectral discrimination was found within the following material classes: red and white ceramic tiles (C01 and C02) 10.6; dark and beige metals (M04 and M08) 9.94; and white and black plastics (P03 and P10) 13.38.

Spectral separability results between different material classes confirm the colour influence regarding spectral reflectance for the wavelengths (400-1000 nm) used

in this study. These results emphasize that VIS-NIR spectral reflectance data might not be spectrally distinct enough to accurately map materials of similar colour.

Low discrimination is especially obvious for dark plastics, gravels, and grey concrete tile roofs, as Herold et al. (2004) found. These classes are spectrally similar, implying potential difficulty in mapping them. Spectral similarity has already been observed in their spectral signatures of nearly constant low reflectance through the VIS-NIR spectral range. In this regard, the use of SWIR spectroscopy that is best suited for several sets of minerals, clays, carbonates and sulphates or silicates and carbonates in TIR and a deeper separability analysis using other metrics, for example, the Bhattacharyya distance (B-distance), could be useful in future works (Herold et al. 2004).

5. Conclusions

Roofs are made from a variety of materials that provide diverse spectral characteristics. A laboratory-based framework to obtain reflectance data using an HSR airborne sensor was described.

Characteristics in the spectral signatures could be identified depending on the composition of the materials. However, colour and surface finishing influence the spectral reflectance for visible wavelengths, making the distinction between materials difficult in some cases.

Materials such as concrete, fibre cement and metals presented similar (flat) spectral signatures. The plastic materials presented a particular spectral signature compared to that of the rest of the materials, especially in the NIR spectral range.

The spectral signatures of roof materials provided qualitative results of their separability. In addition, a quantitative evaluation of spectral discrimination was provided by using RMS. Roof materials, especially those with similar colours within the

same material class and some between different classes, are not spectrally distinct over the VIS-NIR spectral range (400-1000 nm) and may have limitations in regard to discrimination and accurate mapping.

In this regard, work in the SWIR (Herold et al. 2004) and TIR spectral regions could improve the differentiation between roof materials, as Kotthaus et al. (2014) concluded.

It was confirmed that view angles (IFOVs) modify the overall amplitude of reflectance signatures but do not significantly modify spectral shapes.

Although this investigation has shown some limitations for the discrimination between some roof materials, the results showed great potential to obtain reflectance data using the described methodology and an HSR sensor in the laboratory.

The spectral library provides spectral information about common roof materials. Furthermore, it includes new building materials (e.g., plastics and metals) that are underrepresented in the existing spectral libraries. However, due to the large size of the Mediterranean region, more work is still required to represent roof materials according to this geographic region.

The spectral signatures of roof materials considering ageing processes as well as a deeper spectral separability analysis using other metrics, for example, B-distance, should be explored in future works.

Disclosure statement

No potential conflicts of interest were reported by the authors.

Acknowledgements

This work is part of the Fertilecity II project supported by the Spanish Ministry of Economy and Competitiveness (CTM2016-75772-C3-3-R and CTM2016-75772-C3-1-R, AEI/FEDER, UE); from the Spanish Ministry of Science, Innovation and Universities; through the María de

Maeztu program for Units of Excellence (MDM-2015-0552). Authors want to thank to the University of Guadalajara (Mexico) for awarding a research scholarship to Perla Zambrano-Prado, and to the reviewers for their valuable comments.

References

- Alamús, R., F. Pérez, L. Pipia, and J. Corbera. 2018. "Urban Sustainable Ecosystems Assessment through Airborne Earth Observation: Lessons Learned." *International Archives of the Photogrammetry, Remote Sensing and Spatial Information Sciences - ISPRS Archives* 42 (1): 5–10. doi:10.5194/isprs-archives-XLII-1-5-2018.
- Arnold, Chester, and James Gibbons. 1996. "Impervious Surface Coverage: The Emergence of a Key Environmental Indicator." *Journal of the American Planning Association* 62 (2). doi:10.1080/01944369608975688.
- Bayrakci Boz, Mesude, Kirby Calvert, and Jeffrey R. S. Brownson. 2015. "An Automated Model for Rooftop PV Systems Assessment in ArcGIS Using LIDAR." *AIMS Energy* 3 (3): 401–20. doi:10.3934/energy.2015.3.401.
- Ben-Dor, E., N. Levin, and H. Saaroni. 2001. "A Spectral Based Recognition of the Urban Environment Using the Visible and near-Infrared Spectral Region (0.4-1.1 Mm). A Case Study over Tel-Aviv, Israel." *International Journal of Remote Sensing* 22 (11): 2193–2218. doi:10.1080/01431160117759.
- Berger, D. 2013. "A GIS Suitability Analysis of the Potential for Rooftop Agriculture in New York City." Columbia University. <https://academiccommons.columbia.edu/catalog/ac:162285>.
- Brito, M.C., N. Gomes, T. Santos, and J.A. Tenedório. 2012. "Photovoltaic Potential in a Lisbon Suburb Using LiDAR Data." *Solar Energy* 86 (1). Pergamon: 283–88. doi:10.1016/J.SOLENER.2011.09.031.
- Carter, Timothy, and Andrew Keeler. 2008. "Life-Cycle Cost-Benefit Analysis of Extensive Vegetated Roof Systems." *Journal of Environmental Management* 87 (3): 350–63. doi:10.1016/j.jenvman.2007.01.024.
- Castellanos, López L. 1996. *Cubiertas Y Tejados. Manual Práctico*. Madrid: Artes Gráficas Gala.

- Chueca, Pilar. 2003. *Roofs Architecture in Detail*. Barcelona: Links Internacional.
- Farreny, Ramon, Tito Morales-Pinzón, Albert Guisasola, Carlota Tayà, Joan Rieradevall, and Xavier Gabarrell. 2011. "Roof Selection for Rainwater Harvesting: Quantity and Quality Assessments in Spain." *Water Research* 45 (10): 3245–54. doi:10.1016/j.watres.2011.03.036.
- Grant, Aneurin Thomas James, Nathan L. McKinney, and Robert Ries. 2017. "An Approach to Quantifying Rainwater Harvesting Potential Using Imagery, Geographic Information Systems (GIS) and LiDAR Data." *Water Science and Technology: Water Supply* 2012: ws2017026. doi:10.2166/ws.2017.026.
- Hapke, Bruce. 2012. *Theory of Reflectance and Emittance Spectroscopy*. Second. Cambridge: Cambridge University Press. doi:10.1017/CBO9781139025683.
- Heiden, Uta, Sigrid Roessner, Karl Segl, and Hermann Kaufmann. 2001. "Analysis of Spectral Signatures of Urban Surfaces for Their Identification Using Hyperspectral HyMap Data." *IEEE/ISPRS Joint Workshop on Remote Sensing and Data Fusion over Urban Areas (Cat. No.01EX482)*, 173–77. doi:10.1109/DFUA.2001.985871.
- Heiden, Uta, Karl Segl, Sigrid Roessner, and Hermann Kaufmann. 2007. "Determination of Robust Spectral Features for Identification of Urban Surface Materials in Hyperspectral Remote Sensing Data." *Remote Sensing of Environment* 111 (4): 537–52. doi:10.1016/j.rse.2007.04.008.
- Hermiyanty, Wandira Ayu Bertin, Dewi Sinta. 2017. *Remote Sensing and Image Interpretation. Journal of Chemical Information and Modeling*. Vol. 8. doi:10.1017/CBO9781107415324.004.
- Herold, Martin, Dar A. Roberts, Margaret E. Gardner, and Philip E. Dennison. 2004. "Spectrometry for Urban Area Remote Sensing - Development and Analysis of a Spectral Library from 350 to 2400 Nm." *Remote Sensing of Environment* 91 (3–4): 304–19. doi:10.1016/j.rse.2004.02.013.
- IRENA. 2015. "Renewable Energy in the Water Energy & Food Nexus." *International Renewable Energy Agency*. <http://www.irena.org/publications/2015/Jan/Renewable-Energy-in-the-Water-Energy--Food-Nexus>.

- Jamal, Taskin, Weerakorn Ongsakul, Jay Govind Singh, Sayedus Salehin, and S.M. Ferdous. 2014. "Potential Rooftop Distribution Mapping Using Geographic Information Systems (GIS) for Solar PV Installation: A Case Study for Dhaka, Bangladesh." *2014 3rd International Conference on the Developments in Renewable Energy Technology (ICDRET)*. United International University (UIU), 1–6. doi:10.1109/icdret.2014.6861648.
- Jilge, Marianne, Uta Heiden, Martin Habermeyer, André Mende, and Carsten Juergens. 2017. "Detecting Unknown Artificial Urban Surface Materials Based on Spectral Dissimilarity Analysis." *Sensors (Switzerland)* 17 (8). doi:10.3390/s17081826.
- Khan, Jibran, and Mudassar Hassan Arsalan. 2016. "Estimation of Rooftop Solar Photovoltaic Potential Using Geo-Spatial Techniques: A Perspective from Planned Neighborhood of Karachi – Pakistan." *Renewable Energy* 90 (May). Pergamon: 188–203. doi:10.1016/J.RENENE.2015.12.058.
- Kodysh, Jeffrey B., Olufemi A. Omitaomu, Budhendra L. Bhaduri, and Bradley S. Neish. 2013. "Methodology for Estimating Solar Potential on Multiple Building Rooftops for Photovoltaic Systems." *Sustainable Cities and Society* 8. Elsevier B.V.: 31–41. doi:10.1016/j.scs.2013.01.002.
- Kotthaus, Simone, Thomas E.L. Smith, Martin J. Wooster, and C. S.B. Grimmond. 2014. "Derivation of an Urban Materials Spectral Library through Emittance and Reflectance Spectroscopy." *ISPRS Journal of Photogrammetry and Remote Sensing* 94. International Society for Photogrammetry and Remote Sensing, Inc. (ISPRS): 194–212. doi:10.1016/j.isprsjprs.2014.05.005.
- Liu, Jian Guo, and Philippa J Mason. 2009. *Essential Image Processing and GIS for Remote Sensing*. Wiley-Blackwell.
- Lupia, Flavio, Valerio Baiocchi, Ketil Lelo, and Giuseppe Pulighe. 2017. "Exploring Rooftop Rainwater Harvesting Potential for Food Production in Urban Areas." *Agriculture* 7 (6): 46. doi:10.3390/agriculture7060046.
- Margolis, Robert, Pieter Gagnon, Jennifer Melius, Caleb Phillips, and Ryan Elmore. 2017. "Using GIS-Based Methods and Lidar Data to Estimate Rooftop Solar Technical Potential in US Cities." *Environmental Research Letters* 12 (7). doi:10.1088/1748-9326/aa7225.

- Markelin, Lauri, Eija Honkavaara, Jouni Peltoniemi, Eero Ahokas, Risto Kuittinen, Juha Hyypä, Juha Suomalainen, and Antero Kukko. 2008. "Radiometric Calibration and Characterization of Large-Format Digital Photogrammetric Sensors in a Test Field." *Photogrammetric Engineering and Remote Sensing* 74 (12): 1487–1500. doi:10.14358/PERS.74.12.1487.
- Martín, Ana M, Javier Domínguez, and Julio Amador. 2015. "Applying LIDAR Datasets and GIS Based Model to Evaluate Solar Potential over Roofs : A Review" 3 (3): 326–43. doi:10.3934/energy.2015.3.326.
- Milton, Edward J., Nigel P. Fox, and Michael E. Schaepman. 2006. "Progress in Field Spectroscopy." *International Geoscience and Remote Sensing Symposium (IGARSS)* 113. Elsevier Inc.: 1966–68. doi:10.1109/IGARSS.2006.509.
- Nadal, Ana, Ramón Alamús, Luca Pipia, Antonio Ruiz, Jordi Corbera, Eva Cuerva, Joan Rieradevall, and Alejandro Josa. 2017. "Urban Planning and Agriculture. Methodology for Assessing Rooftop Greenhouse Potential of Non-Residential Areas Using Airborne Sensors." *Science of the Total Environment* 601–602. Elsevier B.V.: 493–507. doi:10.1016/j.scitotenv.2017.03.214.
- Nadal, Ana, Daniel Rodríguez-Cadena, Oriol Pons, Eva Cuerva, Alejandro Josa, and Joan Rieradevall. 2019. "Feasibility Assessment of Rooftop Greenhouses in Latin America. The Case Study of a Social Neighborhood in Quito, Ecuador." *Urban Forestry & Urban Greening* 44 (August). Urban & Fischer: 126389. doi:10.1016/J.UFUG.2019.126389.
- Nasarudin, Nurul Ezaty Mohd, and Helmi Zulhaidi Mohd Shafri. 2011. "Development and Utilization of Urban Spectral Library for Remote Sensing of Urban Environment." *Journal of Urban and Environmental Engineering* 5 (1): 44–56. doi:10.4090/juee.2011.v5n1.044056.
- Nguyen, Ha T., Joshua M. Pearce, Rob Harrap, Gerald Barber, Ha T. Nguyen, Joshua M. Pearce, Rob Harrap, and Gerald Barber. 2012. "The Application of LiDAR to Assessment of Rooftop Solar Photovoltaic Deployment Potential in a Municipal District Unit." *Sensors* 12 (4). Molecular Diversity Preservation International: 4534–58. doi:10.3390/s120404534.
- Nidamanuri, Rama Rao, and A. M. Ramiya. 2014. "Spectral Identification of Materials by Reflectance Spectral Library Search." *Geocarto International* 29 (6): 609–24.

doi:10.1080/10106049.2013.821175.

- Ojwang, Robert O., Jörg Dietrich, Prajna Kasargodu Anebagilu, Matthias Beyer, and Franz Rottensteiner. 2017. "Rooftop Rainwater Harvesting for Mombasa: Scenario Development with Image Classification and Water Resources Simulation." *Water (Switzerland)* 9 (5). doi:10.3390/w9050359.
- Orsini, Francesco, Mattia Accorsi, Paulo Luz, I. Tsirogiannis, and Giorgio Gianquinto. 2016. "Sustainable Water Management in Green Roofs." In *Sustainable Water Management in Urban Environments*, 167–207. Springer, Cham. doi:10.1007/978-3-319-29337-0.
- Oyedayo, Oyelowo. 2018. "Spatiotemporal Modelling of Rooftop Rainwater Harvesting with Lidar Data in the Taia Hills, Kenya." University of Helsinki.
- Palmer, Diane, Elena Koumpli, Ian Cole, Ralph Gottschalg, Thomas Betts, Diane Palmer, Elena Koumpli, Ian Cole, Ralph Gottschalg, and Thomas Betts. 2018. "A GIS-Based Method for Identification of Wide Area Rooftop Suitability for Minimum Size PV Systems Using LiDAR Data and Photogrammetry." *Energies* 11 (12). Multidisciplinary Digital Publishing Institute: 3506. doi:10.3390/en11123506.
- Radzali, Nour Ain Mohd, Helmi Zulhaidi Mohd Shafri, Michel Jhon Norman, and Safwan Saufi. 2018. "Roofing Assessment for Rooftop Rainwater Harvesting Adoption Using Remote Sensing and GIS Approach." *International Archives of the Photogrammetry, Remote Sensing and Spatial Information Sciences - ISPRS Archives* 42 (4/W9): 129–32. doi:10.5194/isprs-archives-XLII-4-W9-129-2018.
- Roberts, Dar A, and Martin Herold. 2004. "Imaging Spectrometry of Urban Materials." *Infrared Spectroscopy in Geochemistry, Exploration and Remote Sensing, Mineral Association of Canada, Short Course Series* 33 (March): 155–81.
- Saha, Mithun, and Matthew J. Eckelman. 2017. "Growing Fresh Fruits and Vegetables in an Urban Landscape: A Geospatial Assessment of Ground Level and Rooftop Urban Agriculture Potential in Boston, USA." *Landscape and Urban Planning* 165 (August 2016). Elsevier: 130–41. doi:10.1016/j.landurbplan.2017.04.015.
- Samsudin, Sarah Hanim, Helmi Z. M. Shafri, and Alireza Hamedianfar. 2016. "Development of Spectral Indices for Roofing Material Condition Status Detection

- Using Field Spectroscopy and WorldView-3 Data.” *Journal of Applied Remote Sensing* 10 (2): 25021. doi:10.1117/1.jrs.10.025021.
- Sanyé-Mengual, Esther, Ileana Cerón-Palma, Jordi Oliver-Solà, Juan Ignacio Montero, and Joan Rieradevall. 2015. “Integrating Horticulture into Cities: A Guide for Assessing the Implementation Potential of Rooftop Greenhouses (RTGs) in Industrial and Logistics Parks.” *Journal of Urban Technology* 22 (1): 87–111. doi:10.1080/10630732.2014.942095.
- Schunck, Eberhard, Hans Oster, Rainer Barthel, and Kurt Kiessl. 2003. *Roof Construction Manual: Pitched Roofs*. 5th ed. Basel: Birkhauser.
- Shafri, Helmi Z M, Ebrahim Taherzadeh, Shattri Mansor, and Ravshan Ashurov. 2012. “Hyperspectral Remote Sensing of Urban Areas: An Overview of Techniques and Applications.” *Research Journal of Applied Sciences, Engineering and Technology* 4 (11): 1557–65. <http://maxwellsci.com/print/rjaset/v4-1557-1565.pdf>.
- Singh, Rhythm, and Rangan Banerjee. 2015. “ScienceDirect Estimation of Rooftop Solar Photovoltaic Potential of a City.” *Solar Energy* 115. Elsevier Ltd: 589–602. doi:10.1016/j.solener.2015.03.016.
- Stevens, Antoine, Bas van Wesemael, Harm Bartholomeus, Damien Rosillon, Bernard Tychon, and Eyal Ben-Dor. 2008. “Laboratory, Field and Airborne Spectroscopy for Monitoring Organic Carbon Content in Agricultural Soils.” *Geoderma* 144 (1–2). Elsevier: 395–404. doi:10.1016/J.GEODERMA.2007.12.009.
- Toboso-Chavero, Susana, Ana Nadal, Anna Petit-Boix, Oriol Pons, Gara Villalba, Xavier Gabarrell, Alejandro Josa, and Joan Rieradevall. 2018. “Towards Productive Cities: Environmental Assessment of the Food-Energy-Water Nexus of the Urban Roof Mosaic.” *Journal of Industrial Ecology*, November. John Wiley & Sons, Ltd (10.1111). doi:10.1111/jiec.12829.
- United Nations. 2018. “World Urbanization Prospects: The 2018 Revision- Key Factors.” doi:(ST/ESA/SER.A/366).
- Villarreal, Edgar L., and Andrew Dixon. 2005. “Analysis of a Rainwater Collection System for Domestic Water Supply in Ringdansen, Norrköping, Sweden.” *Building and Environment* 40 (9). Pergamon: 1174–84. doi:10.1016/J.BUILDENV.2004.10.018.

- Wang, Hanyun, and Cheng Wang. 2011. "Roof Detection in Lidar Data." *2011 International Workshop on Multi-Platform/Multi-Sensor Remote Sensing and Mapping*. IEEE, 1–5. doi:10.1109/M2RSM.2011.5697372.
- Weng, Qihao. 2012. "Remote Sensing of Impervious Surfaces in the Urban Areas: Requirements, Methods, and Trends." *Remote Sensing of Environment* 117. Elsevier Inc.: 34–49. doi:10.1016/j.rse.2011.02.030.
- Zambrano-Prado, Perla, Alejandro Josa García-Tornel, Joan Rieradevall, Santiago Gasó, and Xavier Gabarrell Durany. 2017. "Spectral Library of Rooftop Urban Materials." <https://ddd.uab.cat/record/196065>.
- Zinzi, Michele. 2010. "Cool Materials and Cool Roofs: Potentialities in Mediterranean Buildings." *Advances in Building Energy Research* 4 (December 2014): 201–66. doi:10.4324/9781849776349.

Appendices

Appendix A. Script developed for processing the radiance data

```
#####
#####
class sampleToAnalyzeAISA(object):
    def __init__(self, angRanges,lin2Wav,lin2Ang,lin2Spec,ID,imgFile,sampleMaskFile,refMaskFile,QCpath):
        # Maps parameters
        self.angleRanges = angRanges # Angular ranges for spectra to be computed
        self.lineToWave = lin2Wav # Relationship between image band coordinate and Wavelength value [nm]
        self.lineToAngle = lin2Ang # Relationship between image pixel coordinate and incidence angle [°]
        self.lineToSpec = lin2Spec # Spectralon(R) spectral response
        # Retrieve additional param
        self.nAngles = len(self.angleRanges)
        self.nBands = self.lineToWave.shape[0]
        self.sampleID = ID
        # Read data & raster images
        self.sensorImage = gdal.Open(imgFile).ReadAsArray() # Image to be processed
        self.sampMask = gdal.Open(sampleMaskFile).ReadAsArray() # ROI defining the sample
        self.refMask = gdal.Open(refMaskFile).ReadAsArray() # ROI defining the reference (Spectralon (R))

        #####
    def getSampleSpectraForAllAngles(self):
        spectra = np.zeros((self.nBands,self.nAngles),dtype=float)
        # Loop over angles
        for index,angleRange in enumerate(self.angleRanges):
            # Retrieve spectrum for a given angle
            spectrum = getVNIRSpectrum(self.sensorImage,self.sampMask,self.refMask, self.lineToWave,self
            .lineToAngle,self.lineToSpec,angleRange)
            # Update spectral array
            spectra[:,index] = spectrum
        return spectra

        #####
    def getVNIRSpectrum(sensorImage,sampleMask,referenceMask,lineToWavelength,lineToAngle,lineToSpec,angleRange):
        # Get the angular mask (Pixels within the current angular range)
        angleMask = computeAngularMask(lineToAngle,angleRange,sensorImage)
        # Get the multiband sample & reference arrays
        sample = sampleMask*angleMask*sensorImage
        reference = referenceMask*angleMask*sensorImage
        # Perform the row (i.e., time) average
        sampleRowSum = sample.sum(axis=1)
        referenceRowSum = reference.sum(axis=1)

        maskSampleRowSum = (sampleMask*angleMask).sum(axis=0)
        maskReferenceRowSum = (referenceMask*angleMask).sum(axis=0)

        sampleRowAvg = sampleRowSum / maskSampleRowSum
        referenceRowAvg = referenceRowSum / maskReferenceRowSum
        # Apply the calibration reference for the spectralone (externally provided)
        referenceRowAvg = np.divide(referenceRowAvg,np.expand_dims(lineToSpec,axis=1))
        # Get the overlapping columns for both sample and reference
        validColsSample = sampleRowAvg!=0
        validColsReference = referenceRowAvg!=0
        validCols = validColsSample*validColsReference
        # Get the corrected sample values
        correctedSample = np.divide(validCols*sampleRowAvg.astype(float),validCols*referenceRowAvg.astype(float))
        validPoints = np.isfinite(correctedSample).astype(int)
        # Get the column (i.e., angle) average
        correctedSampleColSum = np.nan_to_num(correctedSample).sum(axis=1)
        validPointsColSum = validPoints.sum(axis=1)
        spectrum = np.divide(correctedSampleColSum,validPointsColSum)

        return spectrum
```

Appendix B. Available number of pixels for each sample material

Table 1. Available number of pixels for each sample material and IFOV group to obtain the spectral reflectance data and create the spectral signatures.

Material information		Number of pixels			
ID	Material	IFOV 1	IFOV 2	IFOV 3	IFOV 4
C01	Ceramic tiles	108,287	171,314	187,541	161,026
C02	Gres porcelain tiles	124,781	167,183	171,161	162,894
C03	Gres porcelain tiles	123,133	161,437	165,128	147,434
C04	Gres porcelain tiles	142,740	191,260	195,810	179,309
C05	Gres porcelain tiles	116,428	155,965	156,241	162,027
T01	Concrete tiles	52,860	75,027	48,649	2,864
T02	Concrete tiles	84,130	139,138	183,301	203,680
T03	Concrete bricks	58,675	78,583	80,464	0
T04	Corrugated fibre cement shingles	156,623	209,835	214,856	223,893
M01	Steel shingles	86,148	115,410	118,179	123,145
M02	Galvanized steel shingles	883,33	118,341	121,193	112,239
M03	Inox steel shingles	80,808	108,262	110,852	40,147
M04	Aluminium shingles	82,680	110,770	113,420	36,042
M05	Steel shingles with paint	46,344	62,032	63,526	65,516
M06	Copper shingles	81,676	109,412	112,029	102,333
M07	Zinc shingles	81,432	109,098	111,708	17,220
M08	Steel with paint (sandwich panels)	70,310	94,155	96,407	71,841
M09	Aluminium with paint (sandwich panels)	67,651	90,602	92,769	88,533

PT01	Shingles with blue paint	98,991	132,579	135,783	122,037
PT02	Shingles with red paint	96,080	140,407	148,262	128,012
P01	Methacrylate shingles	88,059	117,910	120,803	67,937
P02	Methacrylate shingles	85,956	115,160	114,316	30,311
P03	Methacrylate shingles	85,488	114,532	115,311	39,840
P04	PVC shingles	89,175	119,444	122,301	55,436
P05	Polycarbonate shingles	67,644	90,601	30,762	0
P06	Polycarbonate shingles	38,033	50,997	42,491	0
P07	Polycarbonate shingles	102,241	136,106	118,257	0
P08	Polycarbonate shingles	67,186	89,888	92,127	0
P09	Polycarbonate shingles	70,824	94,886	97,156	0
P10	Synthetic rubber	70,512	94,468	96,728	73,677
P11	Asphalt polymer	103,501	144,597	148,624	154,360
S01	Granite tiles	53,144	65,331	15,404	0
S02	Granite tiles	51,792	69,388	12,214	0
S03	Granite tiles	52,061	58,487	29,247	0
S04	Granite tiles	51,637	65,597	17,171	0
S05	Slate tiles	162,928	218,300	223,523	202,646
S06	Gravel	90,647	121,420	124,329	129,559
S07	Gravel	88,273	118,273	121,123	126,215
W01	Wood shingles	110,704	148,314	151,494	151,594
